THE JOURNAL OF PHYSICAL CHEMISTRY C

Article

Cite This: J. Phys. Chem. C 2019, 123, 963−970

pubs.acs.org/JPCC

Bismuth Enhances the Stability of $CH_3NH_3PbI_3$ (MAPI) Perovskite under High Humidity

Timothy D. Siegler, Daniel W. Houck, Shin Hum Cho, Delia J. Milliron, and Brian A. Korgel*

McKetta Department of Chemical Engineering, Texas Materials Institute, The University of Texas at Austin, Austin, Texas 78712-1062, United States

Supporting Information

ABSTRACT: Methylammonium lead iodide ($CH_3NH_3PbI_3$, MAPI) is a high-performance solar cell material but lacks stability in the presence of humidity. Addition of a few percent bismuth (Bi) as a trivalent cation substitute for Pb (i.e., MAP(Bi)I) leads to enhanced stability under high (90%) relative humidity (RH). At moderate humidity (60% RH), however, MAP(Bi)I degrades more rapidly than MAPI. Bi incorporation into MAPI either stabilizes or destabilizes the two hydration products, MAPI·H_2O and PbI_2, depending on the amount of humidity in the environment.

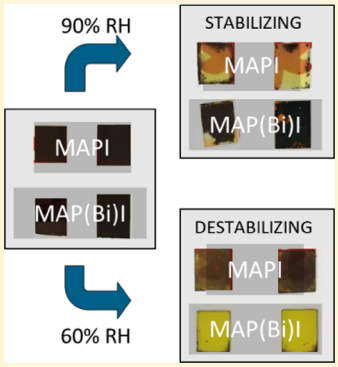

INTRODUCTION

Methylammonium lead iodide ($CH_3NH_3PbI_3$, MAPI) is a hybrid organic−inorganic perovskite (HOIP) and a promising semiconductor for photovoltaic devices (PVs),[1,2] light-emitting diodes (LEDs),[3−5] lasers,[3,4] photocatalytic systems,[6] and γ ray detectors.[7] However, MAPI is highly susceptible to degradation under humidity,[8,9] with the reversible formation of monohydrate and dihydrate species and a final irreversible degradation into PbI_2 via the following reaction pathway[8,10−14]

$$CH_3NH_3PbI_{3(s)} + H_2O_{(g)} \rightleftharpoons CH_3NH_3PbI_3{\cdot}H_2O_{(s)} \quad (1)$$

$$4CH_3NH_3PbI_3{\cdot}H_2O_{(s)} \rightleftharpoons (CH_3NH_3)_4PbI_6{\cdot}2H_2O_{(s)} + 3PbI_{2(s)} + 2H_2O_{(g)} \quad (2)$$

$$(CH_3NH_3)_4PbI_6{\cdot}2H_2O_{(s)} \rightarrow 4CH_3NH_{2(g)} + 4HI_{(g)} + PbI_{2(s)} + 2H_2O_{(g)} \quad (3)$$

The resulting degradation product of PbI_2 is the only remaining solid material. It is certainly possible to stabilize MAPI up to several months by encapsulation in hydrophobic fluoropolymers or glass;[15,16] yet, higher intrinsic stability would greatly help reach commercial viability.[17]

The intrinsic stability of MAPI can be improved to some extent by replacing MA^+, Pb^{2+}, or I^- with other chemical species, either by bringing the Goldschmidt tolerance factor closer to one,[18,19] improving the film morphology,[20−22] or strengthening hydrogen bonding between organic A site components and the halide moiety.[10,23−25] For example, MA^+ has been replaced with formamidinium (FA^+)[26] or cesium (Cs^+),[18,27,28] and I^- has been replaced with Br^-,[22] Cl^-,[20] thiocyanate,[29,30] or selenide,[31] for enhanced stability. There have also been numerous reports detailing the substitution of Pb^{2+} with other species, but most of these do not mention the resulting stability of the materials. The addition of In^{3+} has been shown to stabilize $CH_3NH_3PbI_{3-x}Cl_x$ PVs stored on a benchtop,[32] and the addition of Sr^{2+} to $CsPbI_2Br$ significantly improved the stability of encapsulated PVs stored at <50% RH in the dark.[33] Improved benchtop stability of PVs has been reported for $CH_3NH_3Pb_{0.95}Sn_{0.05}I_3$ devices with added CuBr and MAPI devices with added Co.[34,35]

The additions of Bi,[19,21,36] Sr,[37] and Eu[38] have also been shown to stabilize the cubic perovskite α-phase of $CsPbI_3$[19,36−38] and $FAPbI_3$[21] at room temperature. The equilibrium phase of these materials at room temperature is the orthorhombic nonperovskite δ-phase. It has been proposed that these additives enhance the stability of the cubic perovskite phase by either modifying the tolerance factor,[19,36] increasing microstrain due to a reduced crystal size,[38] or by providing resistance to degradation in the presence of water vapor,[21] since water vapor catalyzes the α-to-δ phase transition.[39] Lehner et al.[40] suggested that $A_3Bi_2I_9$ (A = K, Rb, Cs) compounds, in general, are more durable than their lead perovskite analogues and have observed unchanging X-ray diffraction (XRD) patterns from samples stored for months in air (although the storage conditions were not specified, i.e., humidity level, lighting conditions, and no direct comparison

Received: December 5, 2018
Revised: December 10, 2018
Published: December 14, 2018

DOI: 10.1021/acs.jpcc.8b11674
J. Phys. Chem. C 2019, 123, 963−970

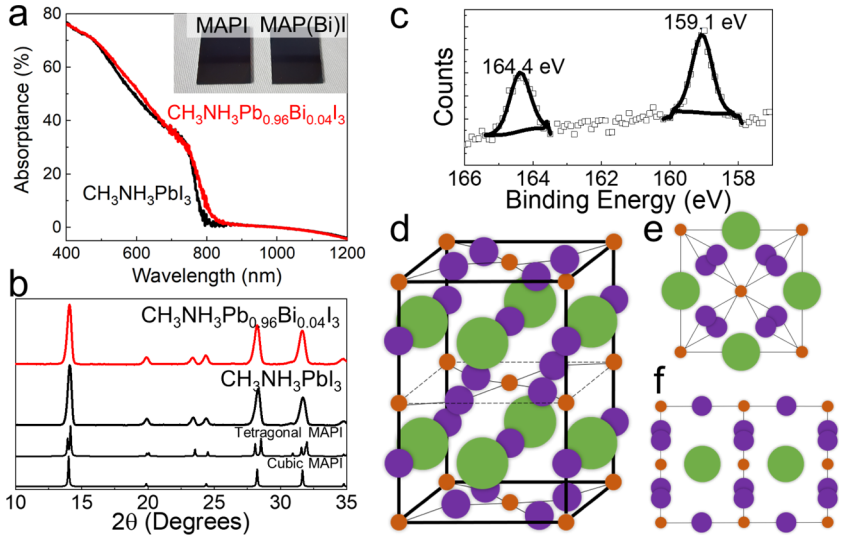

Figure 1. (a) Room-temperature UV−vis absorptance spectra of $CH_3NH_3Pb_{0.96}Bi_{0.04}I_3$ and $CH_3NH_3PbI_3$ films with a similar thickness of 400 nm. Inset: photographs of MAPI (left) and MAP(Bi)I (right) films on APTES-coated glass. (b) XRD of $CH_3NH_3Pb_{0.96}Bi_{0.04}I_3$ (MAP(Bi)I) and $CH_3NH_3PbI_3$ (MAPI) films alongside reference patterns taken from the Crystallography Open Database (COD) for tetragonal and cubic phase MAPI films (COD #4124388 and #4335634, respectively), showing that both films are single-phase tetragonal MAPI films (PDF #01-083-7582) with no noticeable peak shifts or secondary phases upon bismuth incorporation. (c) Bi 4f XPS of $CH_3NH_3Pb_{0.96}Bi_{0.04}I_3$, with peak positions of the fitted Gaussian−Lorentzian function labeled. Data are represented by the hollow points, whereas fitted Gaussian−Lorentzian functions are shown as the thin lines. These peaks are characteristic of Bi^{3+}, and peak integration gives a Bi/Pb molar ratio of 0.04:1. XPS data for the other elements are provided in Supporting Information. (d) Tetragonal crystal structure of methylammonium lead iodide and projections of MAPI viewed down the (e) ⟨001⟩ and (f) ⟨100⟩ directions. Methylammonium atoms are large green circles, iodide ions are moderately sized purple circles, and lead ions are small orange circles.

between the stability of $A_3Bi_2I_9$ and MAPI was made). Another recent paper reported PVs of $FA_{0.83}MA_{0.17}Pb(I_{0.83}Br_{0.17})_3$ mixed with $MA_3Bi_2Br_9$ that demonstrated better thermal stability and comparable humidity stability as single-phase $FA_{0.83}MA_{0.17}Pb(I_{0.83}Br_{0.17})_3$.[41]

Inspired by this previous work, we explored the addition of Bi as a route for stabilizing MAPI in the presence of humidity. We find that partial substitution of Pb^{2+} with Bi^{3+} can either stabilize or destabilize MAPI, depending on the relative humidity (RH). Under high relative humidity (RH = 90%), the addition of a few percent of Bi^{3+} significantly reduces the rate of degradation of MAPI. However, under moderate humidity (RH = 60%), added Bi^{3+} significantly increases the rate of degradation. We propose that the added Bi^{3+} accelerates and decelerates different reaction pathways involved in the degradation of MAPI, which results in stabilization or degradation of MAP(Bi)I depending on the amount of moisture in the environment.

EXPERIMENTAL DETAILS

Materials. Lead iodide (PbI_2, 99.999% ultradry, Alfa Aesar), bismuth iodide (BiI_3, 99.998% ultradry, Alfa Aesar), methylammonium iodide (CH_3NH_3I, MAI, Dye-Sol), anhydrous diethyl ether ($(CH_3CH_2)_2O$, anhydrous >99.0%, BHT inhibitor, Sigma), anhydrous dimethyl sulfoxide ($(CH_3)_2SO$, anhydrous 99.9%, Sigma), anhydrous dimethylformamide ($HCON(CH_3)_2$, 99.8% Sigma), ethanol (CH_3CH_2OH, 200 proof, Fisher Scientific), glycerol ($HOCH_2CH(OH)CH_2OH$, 98%, Fisher Scientific), and (3-aminopropyl)triethyoxysilane ($H_2N(CH_2)_3Si(OC_2H_5)_3$, >98%, Sigma) were all used as received.

Preparation of MAPI and MAP(Bi)I. Glass substrates (1″ × 1″, Cardinal Glass) were sonicated in ethanol for 30 min and immersed in (3-aminopropyl)triethoxysilane (APTES) in ethanol (1:9 APTES/ethanol vol ratio) for 5 min. A drop of water was added to the APTES solution to promote APTES grafting. The substrates were rinsed with IPA and heated at 100 °C in ambient air for 10 min.

Smooth perovskite films were deposited on glass substrates using a modification of the procedure developed by Park et al.[42] A MAPI precursor solution was dissolved by adding 273 mg of PbI_2, 95 mg of MAI, and 120 mL of dimethyl sulfoxide (DMSO) to 480 mL of dimethylformamide (DMF) and stirring at room temperature for 2 h. The resultant solution had a 1:1 molar ratio of PbI_2/MAI. Likewise, 356 mg of BiI_3, 95 mg of MAI, and 120 mL of DMSO were dissolved in 480 mL of DMF in a separate vial, forming a 1:1 molar ratio BiI_3/MAI. After 2 h of stirring, to generate the MAP(Bi)I precursor solution, the lead-based solution was mixed with the bismuth-based solution in a 19:1 ratio by volume (5 mol % Bi on a metal basis), forming a solution with a 0.95:0.05:1 PbI_2/BiI_3/MAI mole ratio.

Spin-coating was performed on glass slides coated with APTES in a nitrogen glovebox with O_2 < 5 ppm. Respective precursor solution (50 μL) was spread evenly over the substrate, and then the substrate was spun at 5000 rpm for 30 s, with a ramp rate of 2500 rpm/s. About 12−15 s into the spin-coating process, ∼500 μL of diethyl ether was dropped onto the substrate, creating smooth, clear, uniform films. Films were immediately annealed at 60 °C for 1 min, then at 100 °C for 2 min. The resulting films were smooth and semi-transparent.

Exposure of MAPI and MAP(Bi)I Perovskite Films to Humidity. Perovskite films were aged in a home-built humidity chamber. Humidity was controlled by mixing water and glycerol in the appropriate ratios and waiting ∼48 h for the mixture to equilibrate with the sealed atmosphere.[10,43] For 90% RH, 28 mL of DI H_2O was mixed with 12 mL of glycerol.

DOI: 10.1021/acs.jpcc.8b11674
J. Phys. Chem. C 2019, 123, 963−970

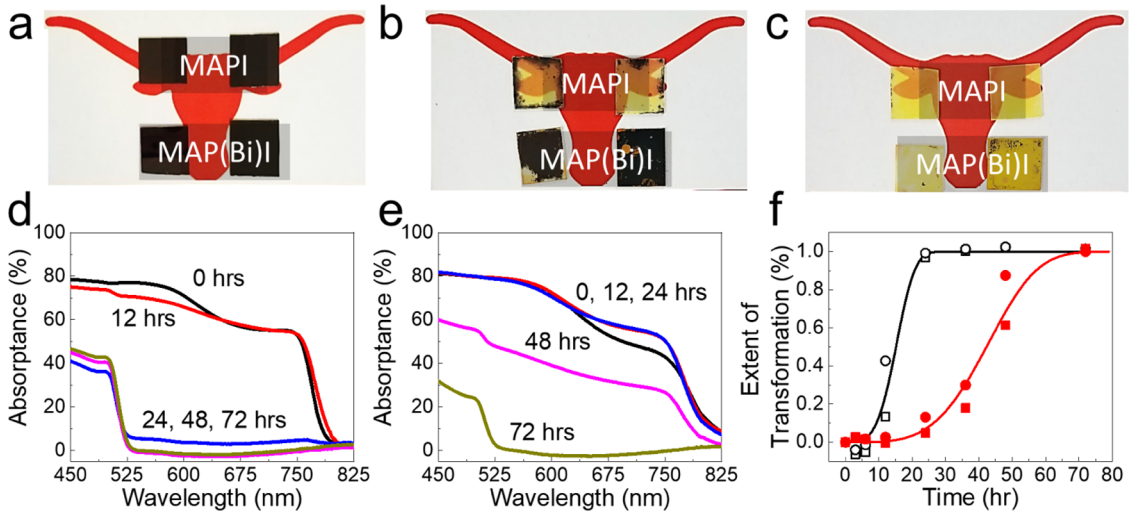

Figure 2. (A–C) Photographs of MAPI and MAP(Bi)I films (A) before and after exposure to 90% RH air under indoor lighting (2 mW/cm^2) for (B) 24 h and (C) 72 h. (d, e) UV–vis absorptance spectra of (d) MAPI and (e) MAP(Bi)I thin films after exposure to air at 90% RH under controlled indoor lighting. (f) Extent of transformation of the (□, ○) MAPI and (red box solid, red circle solid) MAP(Bi)I films as a function of exposure time to 90% RH. The solid lines are the best fits of eq 4 to the MAPI (black line) and MAP(Bi)I (red line) data, with n = 3.9, k = 1.87 × 10^{-5} $h^{-3.9}$ (r^2 = 0.88) and and n = 4.0, k = 2.17 × 10^{-7} $h^{-4.0}$ (r^2 = 0.85), respectively.

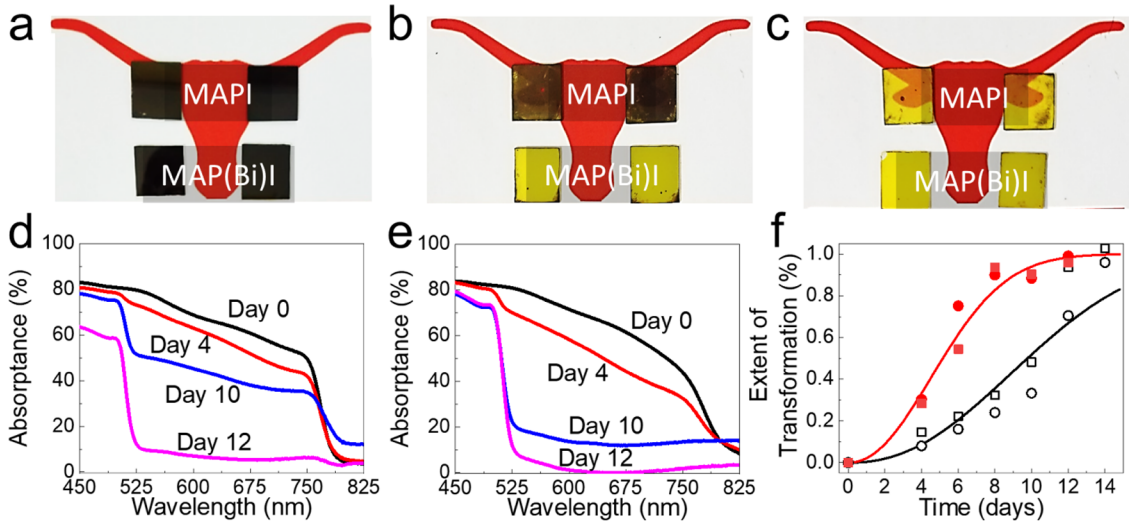

Figure 3. (A–C) Photographs of MAPI and MAP(Bi)I films (A) before and after exposure to air at 60% RH under indoor lighting (2 mW/cm^2) for (B) 8 days, and (C) 14 days. The top row of films in photographs corresponds to MAPI films, whereas the bottom row corresponds to MAP(Bi)I. (D, E) UV–vis absorptance profiles of (D) MAPI and (E) MAP(Bi)I thin films after different aging times at 60% RH in indoor lighting. (F) Plot of the extent of transformation of the (□, ○) MAPI and (red box solid, red circle solid) MAP(Bi)I films. The solid lines are the best fits of eq 4 to the MAPI (black line) and MAP(Bi)I (red line) data, with n = 2.3, k = 3.94 × 10^{-3} $day^{-2.3}$ (r^2 = 0.81) and n = 2.1, k = 2.15 × 10^{-2} $day^{-2.1}$ (r^2 = 0.91), respectively.

For 60% RH, 13.4 mL of DI H_2O was added to 26.6 mL of glycerol. MAPI and MAP(Bi)I films were exposed to humidity under controlled indoor lighting with ∼2 mW/cm^2 total light intensity, as measured by a Newport Optical model 1916-C meter with an 818P-020-12 high power detector. The intensity spectrum of the light source (GE, Starcoat T5 EcoLux High Efficiency & High Output Bulbs, 46705, 3500 K operating temperature) is provided by the manufacturer in their specification sheet.[44]

Materials Characterization. X-ray diffraction (XRD) was carried out using a Rigaku R-Axis Spider X-Ray Diffractometer with an image plate detector and Cu Kα radiation source (λ = 0.154 nm). Samples were probed directly on prepared glass substrates using a flat substrate holder. Scans were performed for 10 min at 5°/s sample rotation under 40 kV and 40 mA radiation.

X-ray photoelectron spectroscopy (XPS) samples were prepared by depositing perovskite films onto a treated fluorinated tin oxide (FTO) glass substrate. The samples were loaded onto the sample holder with copper tape and grounded with conductive carbon tape to minimize charging of the film. Samples were exposed to ultrahigh vacuum for less than 5 h before spectra were taken to eliminate off-gassing of volatile methylamine moieties. XPS spectra were obtained with a Kratos photoelectron spectrophotometer using a monochromatic Al Kα X-ray source and a 180° hemispherical analyzer. The spectra were processed with CasaXPS software. Charging was corrected by shifting the spectra such that the C

DOI: 10.1021/acs.jpcc.8b11674
J. Phys. Chem. C 2019, 123, 963–970

1s peaks are at the expected binding energy of adventitious carbon (284.8 eV). Peak fitting was performed using a Shirley background subtraction and the Gaussian−Lorentzian profile. For composition estimates, each fit peak was integrated and divided by the corresponding relative sensitivity factor in the Kratos library.

Scanning electron microscopy (SEM) images were acquired with a Hitachi S550 SEM/STEM operated at 20 keV in SEM mode. Samples were imaged on FTO glass slides, prepared as described above. Charging was minimized by grounding the sample with conductive carbon tape.

UV−vis−NIR absorptance and absorbance spectroscopy was performed on perovskite films on glass substrates in an Agilent Cary 5000 UV−vis−NIR spectrophotometer. Absorptance was measured by placing samples in an Agilent Diffuse Reflectance Accessory (DRA)-2500 series with a PbS NIR detector and a R928 photomultiplier tube for visible range detection. Spectra were collected in transflectance mode using a center mount holder. Baselines were taken by placing a piece of cleaned glass in the center mount for the 100% T baseline and by blocking the beam at the transmission port of the DRA with aluminum foil for the 0% T baseline. The absorptance, A, is related to the reflectance, R, and the transmittance T, of the film: $A = 1 - R - T$. The absorptance, A, is related to the absorbance $\mathcal{A}$, of the sample as $A = 1 - 10^{-\mathcal{A}}$.[45]

RESULTS AND DISCUSSION

MAPI films were deposited on 3-aminopropyltriethoxysilane (APTES)-treated glass by spin-coating a solution of CH_3NH_3I and PbI_2 in a mixture of DMF and DMSO.[42] Bi^{3+} was incorporated into the films by adding 5 mol % BiI_3 to the solution of CH_3NH_3I and PbI_2. The MAPI and MAP(Bi)I films have similar color, as observed in the photograph in the inset of Figure 1a. Figure 1a compares the UV−vis absorptance spectra of the two films. MAPI exhibits the expected absorption edge at 800 nm (1.5 eV) and absorption plateaus at 580 and 745 nm.[10] The MAP(Bi)I film also exhibits two absorption plateaus near 580 and 745 nm, with a slightly red-shifted absorption edge. A similar red shift has been reported in previous studies on hybrid organic−inorganic perovskites doped with Bi^{3+} and has been attributed to the introduction of shallow trap states that increase the Urbach energy of the material.[46−51] The films in Figure 1a have similar thickness, indicating that the absorption coefficients of the MAPI and MAP(Bi)I are similar, consistent with the expected nature of bismuth doping in hybrid organic−inorganic perovskites.[46−51]

X-ray diffraction (XRD) data in Figure 1b show that the MAPI and MAP(Bi)I films have tetragonal crystal structure, which is the expected room-temperature phase of MAPI.[10,29,46] There is no indication of additional phases in either of the MAPI or MAP(Bi)I films, and the diffraction patterns have similar peak positions, consistent with other studies of aliovalent doping with Bi[46,49,52,53] and other B-site substitutions.[32,54,55] X-ray photoelectron spectroscopy (XPS) also confirmed the presence of Bi in the MAP(Bi)I films. Figure 1c shows XPS from the Bi $4f_{7/2}$ spectral region. These peaks with binding energies between 157 and 161 eV indicate that Bi has a +3 oxidation state,[56] and the Bi 4f to Pb 4f XPS peak ratios show that the Bi/Pb mole ratio in the MAP(Bi)I film is 0.04 (see Supporting Information for XPS of the MAPI films and the Pb 4f, I 3d, and N 1s regions).

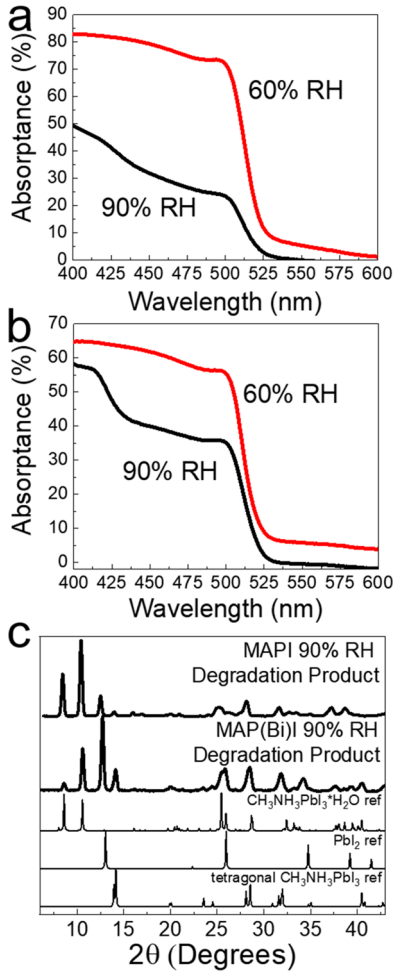

Figure 4. UV−vis absorptance spectroscopy of (a) MAPI and (b) MAP(Bi)I films after exposure to 60% RH for 14 and 12 days, respectively, and 90% RH for 36 h and 3 days, respectively. (c) XRD of the degradation products of MAPI and MAP(Bi)I films exposed to 90% RH. Reference patterns for tetragonal MAPI (COD #4124388, PDF #01-083-7582), PbI_2 (COD #1010062, PDF #00-007-0235), and MAPI monohydrate (COD #7117405) are provided for comparison.

The stability of MAPI and MAP(Bi)I films in the presence of humidity was tested in by monitoring their optical properties over time. Figures 2 and 3 show photographs and optical absorptance spectra of MAPI and MAP(Bi)I films exposed to air for several days at 90 and 60% RH. The humidity was carefully controlled in these experiments using a closed container with appropriate mixtures of water and glycerol.[10] Degraded MAPI films look yellow, with absorptance that decreases between 525 and 800 nm.[8,10] MAPI has an absorption onset at 1.55 eV (800 nm),[10] whereas the degradation products, PbI_2 and MAPI monohydrate, have absorption edges at 2.3 eV (540 nm) and 3.1 eV (400 nm), respectively.[8,10,12,57] Figures 2d,e and 3d,e show the absorptance spectra of MAPI and MAP(Bi)I films changing over time when exposed to air at 90 and 60% RH. The MAPI film has become completely transparent between 525 and 800 nm after only 1 day of exposure to air at 90% RH. MAPI is significantly more stable in 60% RH, and it takes about 12 days for the film to go clear in this wavelength range. Note that these degradation rates are relatively fast because the films were stored under room light, which has been shown to

DOI: 10.1021/acs.jpcc.8b11674
J. Phys. Chem. C 2019, 123, 963−970

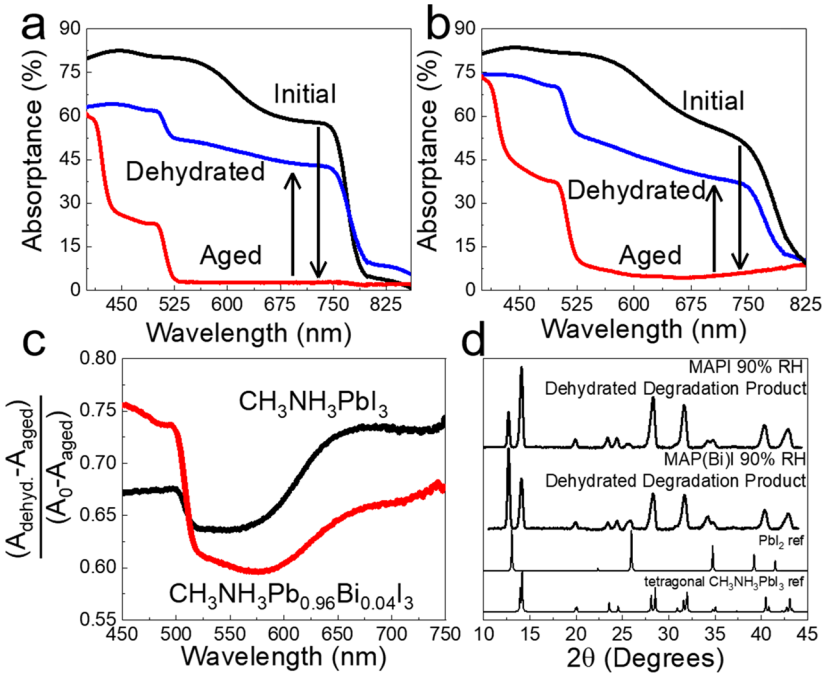

Figure 5. UV−vis absorptance spectra of (A) MAPI and (B) MAP(Bi)I films on glass after 1 cycle of degradation at 90% RH, followed by dehydration with heating at 100 °C in 50% RH air for 2 min. (C) Ratios of the absorptance of MAPI and MAP(Bi)I films before and after exposure to humidity and dehydration $\theta(\lambda)$, calculated using eq 5. (D) XRD of MAPI and MAP(Bi)I films after degrading the MAPI and MAP(Bi)I films to the clear state with exposure to 90% RH air and then dehydration by heating at 100 °C in 50% RH air for 2 min. Peaks matching tetragonal phase of MAPI (COD #4124388, PDF #01-083-7582) are designated with vertical gray lines, whereas dashed yellow lines designate degradation byproduct PbI_2 (COD #1010062, PDF #00-007-0235).

accelerate degradation processes compared to films stored in the dark.[10,58−61] At high humidity (90% RH), the MAP(Bi)I film is significantly more stable than the MAPI film, and it takes 3 days for the film to go clear. In contrast, the MAP(Bi)I film is less stable than the MAPI film at lower humidity of 60% RH, changing from the black tetragonal phase to the yellow degradation product of PbI_2 in only 8 days.

The data in Figures 2 and 3 show that inclusion of bismuth stabilizes MAPI under high humidity (90% RH), while resulting in faster degradation at lower humidity (60% RH). We analyzed the data using an Avrami equation,[62,63]

$$y = 1 - \exp(-kt^n) \quad (4)$$

where k is a rate constant, n is the Avrami exponent, and y is volume fraction converted to degradation product or extent of transformation. The extent of transformation, y, is calculated from the logarithmic absorptance at 600 nm, where $y = [\log(1 - A_{600nm}(t))/\log(1 - A_{600nm}(0))]$. The fits of the Avrami equation (eq 4) to the data in Figures 2f and 3f give Avrami coefficient, n, that are similar for both MAPI and MAP(Bi)I, which are close to 4 for the degradation under high humidity (90% RH) and close to 2 under lower humidity (60% RH). Values of $n = 4$ indicate that MAPI degradation occurs by concurrent nucleation and isotropic growth of domains of degradation product.[63] Values of $n = 2$ indicate that the degradation products form anisotropically, perhaps nucleating and growing initially along grain boundaries.[63] The distinct difference in the values of n is consistent with two different degradation pathways for the films at different humidity conditions. The values of k for the MAPI and MAP(Bi)I films are also significantly higher under lower humidity conditions. The characteristic times for the films to degrade, $\tau = \sqrt[n]{1/k}$, are 16.3 and 46.3 h at RH = 90% and 11.1 and 6.2 days at RH = 60% for the MAPI and MAP(Bi)I films, respectively. To our knowledge, this is the first example of a humidity-specific stability enhancement from compositional engineering in HOIP materials. These values may vary with light exposure,[58−61,64] which could be of interest for future work. Previously observed enhancements in MAPI stability under humidity with various additives have been attributed to the formation of a layered perovskite structure[29,40] or an improved film morphology.[32] These effects reduce the penetration of water vapor into the film and provide enhanced stability under a wide range of humidity. Since Bi addition only stabilizes MAPI at high humidity and actually reduces the stability at lower humidity, it probably does not reduce the rate of water vapor penetration into the film, as in these other cases, but provides enhanced stability for a different reason. Furthermore, the addition of Bi to the MAPI films did not have any obvious effect on the morphology of the film (see Supporting Information for SEM images).

The degradation of MAPI under humid conditions begins by hydration to $CH_3NH_3PbI_3{\cdot}H_2O$. Above ∼75% RH, this monohydrate species is stable and can be detected spectroscopically.[10−13,65] At lower humidity, it spontaneously decomposes, either to (1) $CH_3NH_3PbI_3$ and water vapor (reversion to pristine tetragonal MAPI phase) or to (2) a dihydrate and PbI_2 (leading to further degradation).[8,10,12,13] The absorptance spectra of the MAPI and MAP(Bi)I films in Figure 4a,b all have an absorption onset at 525 nm that is characteristic of PbI_2. The films exposed to high humidity (90% RH) show the additional onset of an absorption feature at 430 nm, which is consistent with MAPI monohydrate.[12,57] XRD (Figure 4c) also shows peaks that correspond to MAPI monohydrate. These observations indicate that degradation at

DOI: 10.1021/acs.jpcc.8b11674
J. Phys. Chem. C 2019, 123, 963−970

90% RH occurs by the reaction pathway shown in eq 1 (monohydrate formation), whereas at 60% RH, the degradation pathway follows eq 2 (dihydrate formation).

To determine the reversibility of the MAPI and MAP(Bi)I degradation reaction and gain insight about the role of Bi in stabilizing the films at high humidity, films were degraded to their clear state by exposure to 0% RH and then heated at 100 °C in air at 50% RH for 2 min to regenerate the dark state. This dehydration step at moderate humidity can also result in further decomposition of the monohydrate to MAPI and PbI_2, as in eq 2. The PbI_2 generated in the dehydration step provides a signature of the relative rate of the reaction in eq 2 for the MAPI and MAP(Bi)I films.[64] This is determined from the ratio of the absorptance of the film before exposure to humidity $A_0(\lambda)$, after exposure $A_{aged}(\lambda)$, and after dehydration $A_{dehyd}(\lambda)$

$$\theta(\lambda) = \frac{A_{dehyd}(\lambda) - A_{aged}(\lambda)}{A_0(\lambda) - A_{aged}(\lambda)} \quad (5)$$

Higher values of $\theta(\lambda)$ between 525 and 800 nm indicate a higher degree of reversion to tetragonal perovskite, and a sharper increase of $\theta(\lambda)$ at 525 nm indicates that more PbI_2 has formed during the heating step at 50% RH. Figure 5a,b shows the absorptance spectra of the MAPI and MAP(Bi)I films, and Figure 5c shows the corresponding values of $\theta(\lambda)$. The MAP(Bi)I films have more PbI_2 after dehydration than the MAPI films. The XRD of the MAPI and MAP(Bi)I films after the heating step, shown in Figure 5d, also shows that more PbI_2 has formed in the film with Bi. This indicates that the rate of reaction for eq 2 is faster when Bi is present in the film. It also explains why MAP(Bi)I is less stable than MAPI when exposed to lower humidity conditions, even though the rate of the reaction in eq 1 is reduced with addition of Bi and leads to slower degradation under high humidity (90% RH).

CONCLUSIONS

In conclusion, the incorporation of Bi into MAPI slows the degradation of the film at high humidity (90% RH). At lower humidity (60% RH), the added Bi enhances the rate of degradation of the film. This is the result of two different degradation pathways, which are either slowed (i.e., eq 1) or enhanced (i.e., eq 2) by the addition of Bi. These results show that partial substitution of Pb in HOIPs may be an effective way to improve stability under humidity; however, more generally, they show that the compositional engineering of HOIPs may lead to differences in stabilization or destabilization that depend on the actual environmental conditions, and film stability should be tested over a range of environmental conditions to determine the overall effect of the additive on the stability of the material.

ASSOCIATED CONTENT

Supporting Information

The Supporting Information is available free of charge on the ACS Publications website at DOI: 10.1021/acs.jpcc.8b11674.

XPS data and SEM images of MAPI and MAP(Bi)I films (PDF)

AUTHOR INFORMATION

Corresponding Author

*E-mail: korgel@che.utexas.edu.

ORCID

Shin Hum Cho: 0000-0002-0271-116X
Delia J. Milliron: 0000-0002-8737-451X
Brian A. Korgel: 0000-0001-6242-7526

Notes

The authors declare no competing financial interest.

ACKNOWLEDGMENTS

The authors acknowledge financial support of this work from the Robert A. Welch Foundation (F-1464, F-1848), the NSF Industry/University Cooperative Research Center on Next Generation Photovoltaics (IIP-1540028 and IIP-1822206), and The Center for Dynamics and Control of Materials (CDCM) Materials Research Science and Engineering Center (MRSEC) supported by the NSF (DMR-1720595). T.D.S. acknowledges support by the United States Government under DoD, Air Force Office of Scientific Research, National Defense Science and Engineering Graduate (NDSEG) Fellowship, 32 CFR 168a. S.H.C. was supported by the NSF (CBET-1704634). We thank Philip Liu for guidance on the APTES treatment and Hugo Celio for assistance with XPS.

REFERENCES

(1) Saliba, M.; Correa-Baena, J.-P.; Grätzel, M.; Hagfeldt, A.; Abate, A. Perovskite Solar Cells: From the Atomic Level to Film Quality and Device Performance. *Angew. Chem., Int. Ed.* **2018**, *57*, 2554−2569.

(2) Unger, E. L.; Kegelmann, L.; Suchan, K.; Sörell, D.; Korte, L.; Albrecht, S. Roadmap and Roadblocks for the Band Gap Tunability of Metal Halide Perovskites. *J. Mater. Chem. A* **2017**, *5*, 11401−11409.

(3) Adjokatse, S.; Fang, H.-H.; Loi, M. A. Broadly Tunable Metal Halide Perovskites for Solid-State Light-Emission Applications. *Mater. Today* **2017**, *20*, 413−424.

(4) Veldhuis, S. A.; Boix, P. P.; Yantara, N.; Li, M.; Sum, T. C.; Mathews, N.; Mhaisalkar, S. G. Perovskite Materials for Light-Emitting Diodes and Lasers. *Adv. Mater.* **2016**, *28*, 6804−6834.

(5) Zhang, Q.; Su, R.; Du, W.; Liu, X.; Zhao, L.; Ha, S. T.; Xiong, Q. Advances in Small Perovskite-Based Lasers. *Small Methods* **2017**, *1*, No. 1700163.

(6) Chen, Y.-S.; Manser, J. S.; Kamat, P. V. All Solution-Processed Lead Halide Perovskite-$BiVO_4$ Tandem Assembly for Photolytic Solar Fuels Production. *J. Am. Chem. Soc.* **2015**, *137*, 974−981.

(7) Yakunin, S.; Dirin, D. N.; Shynkarenko, Y.; Morad, V.; Cherniukh, I.; Nazarenko, O.; Kreil, D.; Nauser, T.; Kovalenko, M. V. Detection of Gamma Photons Using Solution-Grown Single Crystals of Hybrid Lead Halide Perovskites. *Nat. Photonics* **2016**, *10*, 585−589.

(8) Manser, J. S.; Saidaminov, M. I.; Christians, J. A.; Bakr, O. M.; Kamat, P. V. Making and Breaking of Lead Halide Perovskites. *Acc. Chem. Res.* **2016**, *49*, 330−338.

(9) Berhe, T. A.; Su, W.-N.; Chen, C.-H.; Pan, C.-J.; Cheng, J.-H.; Chen, H.-M.; Tsai, M.-C.; Chen, L.-Y.; Dubale, A. A.; Hwang, B.-J. Organometal Halide Perovskite Solar Cells: Degradation and Stability. *Energy Environ. Sci.* **2016**, *9*, 323−356.

(10) Christians, J. A.; Miranda Herrera, P. A.; Kamat, P. V. Transformation of the Excited State and Photovoltaic Efficiency of $CH_3NH_3PbI_3$ Perovskite upon Controlled Exposure to Humidified Air. *J. Am. Chem. Soc.* **2015**, *137*, 1530−1538.

(11) Müller, C.; Glaser, T.; Plogmeyer, M.; Sendner, M.; Döring, S.; Bakulin, A. A.; Brzuska, C.; Scheer, R.; Pshenichnikov, M. S.; Kowalsky, W.; et al. Water Infiltration in Methylammonium Lead Iodide Perovskite: Fast and Inconspicuous. *Chem. Mater.* **2015**, *27*, 7835−7841.

(12) Leguy, A. M. A.; Hu, Y.; Campoy-Quiles, M.; Alonso, M. I.; Weber, O. J.; Azarhoosh, P.; van Schilfgaarde, M.; Weller, M. T.; Bein, T.; Nelson, J.; et al. Reversible Hydration of $CH_3NH_3PbI_3$ in Films, Single Crystals, and Solar Cells. *Chem. Mater.* **2015**, *27*, 3397−3407.

DOI: 10.1021/acs.jpcc.8b11674
J. Phys. Chem. C 2019, 123, 963−970

(13) Schlipf, J.; Bießmann, L.; Oesinghaus, L.; Berger, E.; Metwalli, E.; Lercher, J. A.; Porcar, L.; Müller-Buschbaum, P. In Situ Monitoring the Uptake of Moisture into Hybrid Perovskite Thin Films. *J. Phys. Chem. Lett.* **2018**, *9*, 2015−2021.
(14) Ciccioli, A.; Latini, A. Thermodynamics and the Intrinsic Stability of Lead Halide Perovskites $CH_3NH_3PbX_3$. *J. Phys. Chem. Lett.* **2018**, *9*, 3756−3765.
(15) Bella, F.; Griffini, G.; Correa-Baena, J.-P.; Saracco, G.; Grätzel, M.; Hagfeldt, A.; Turri, S.; Gerbaldi, C. Improving Efficiency and Stability of Perovskite Solar Cells with Photocurable Fluoropolymers. *Science* **2016**, *354*, 203−206.
(16) Zhou, Y.; Zhu, K. Perovskite Solar Cells Shine in the "Valley of the Sun.". *ACS Energy Lett.* **2016**, *1*, 64−67.
(17) Woodhouse, M.; Jones-Albertus, R.; Feldman, D.; Fu, R.; Horowitz, K.; Chung, D.; Jordan, D.; Kurtz, S. *On the Path to SunShot: The Role of Advancements in Solar Photovoltaic Efficiency, Reliability, and Cost*; National Renewable Energy Laboratory: Golden, CO, 2016. http://www.nrel.gov/docs/fy16osti/65872.pdf (accessed Jan 3, 2018).
(18) Li, Z.; Yang, M.; Park, J.-S.; Wei, S.-H.; Berry, J. J.; Zhu, K. Stabilizing Perovskite Structures by Tuning Tolerance Factor: Formation of Formamidinium and Cesium Lead Iodide Solid-State Alloys. *Chem. Mater.* **2016**, *28*, 284−292.
(19) Hu, Y.; Bai, F.; Liu, X.; Ji, Q.; Miao, X.; Qiu, T.; Zhang, S. Bismuth Incorporation Stabilized α-$CsPbI_3$ for Fully Inorganic Perovskite Solar Cells. *ACS Energy Lett.* **2017**, *2*, 2219−2227.
(20) Chae, J.; Dong, Q.; Huang, J.; Centrone, A. Chloride Incorporation Process in $CH_3NH_3PbI_{3-x}Cl_x$ Perovskites via Nanoscale Bandgap Maps. *Nano Lett.* **2015**, *15*, 8114−8121.
(21) Hu, Y.; Qiu, T.; Bai, F.; Miao, X.; Zhang, S. Enhancing Moisture-Tolerance and Photovoltaic Performances of $FAPbI_3$ by Bismuth Incorporation. *J. Mater. Chem. A* **2017**, *5*, 25258−25265.
(22) Noh, J. H.; Im, S. H.; Heo, J. H.; Mandal, T. N.; Seok, S. I. Chemical Management for Colorful, Efficient, and Stable Inorganic−Organic Hybrid Nanostructured Solar Cells. *Nano Lett.* **2013**, *13*, 1764−1769.
(23) Quarti, C.; Grancini, G.; Mosconi, E.; Bruno, P.; Ball, J. M.; Lee, M. M.; Snaith, H. J.; Petrozza, A.; Angelis, F. D. The Raman Spectrum of the $CH_3NH_3PbI_3$ Hybrid Perovskite: Interplay of Theory and Experiment. *J. Phys. Chem. Lett.* **2014**, *5*, 279−284.
(24) Yamamoto, K.; Iikubo, S.; Yamasaki, J.; Ogomi, Y.; Hayase, S. Structural Stability of Iodide Perovskite: A Combined Cluster Expansion Method and First-Principles Study. *J. Phys. Chem. C* **2017**, *121*, 27797−27804.
(25) Ke, J. C. R.; Walton, A. S.; Lewis, D. J.; Tedstone, A.; O'Brien, P.; Thomas, A. G.; Flavell, W. R. In Situ Investigation of Degradation at Organometal Halide Perovskite Surfaces by X-Ray Photoelectron Spectroscopy at Realistic Water Vapour Pressure. *Chem. Commun.* **2017**, *53*, 5231−5234.
(26) Li, W.-G.; Rao, H.-S.; Chen, B.-X.; Wang, X.-D.; Kuang, D.-B. A Formamidinium−Methylammonium Lead Iodide Perovskite Single Crystal Exhibiting Exceptional Optoelectronic Properties and Long-Term Stability. *J. Mater. Chem. A* **2017**, *5*, 19431−19438.
(27) Kulbak, M.; Gupta, S.; Kedem, N.; Levine, I.; Bendikov, T.; Hodes, G.; Cahen, D. Cesium Enhances Long-Term Stability of Lead Bromide Perovskite-Based Solar Cells. *J. Phys. Chem. Lett.* **2016**, *7*, 167−172.
(28) Saliba, M.; Matsui, T.; Seo, J.-Y.; Domanski, K.; Correa-Baena, J.-P.; Nazeeruddin, M. K.; Zakeeruddin, S. M.; Tress, W.; Abate, A.; Hagfeldt, A.; et al. Cesium-Containing Triple Cation Perovskite Solar Cells: Improved Stability, Reproducibility and High Efficiency. *Energy Environ. Sci.* **2016**, *9*, 1989−1997.
(29) Jiang, Q.; Rebollar, D.; Gong, J.; Piacentino, E. L.; Zheng, C.; Xu, T. Pseudohalide-Induced Moisture Tolerance in Perovskite $CH_3NH_3Pb(SCN)_2$ I Thin Films. *Angew. Chem., Int. Ed.* **2015**, *54*, 7617−7620.
(30) Tai, Q.; You, P.; Sang, H.; Liu, Z.; Hu, C.; Chan, H. L. W.; Yan, F. Efficient and Stable Perovskite Solar Cells Prepared in Ambient Air Irrespective of the Humidity. *Nat. Commun.* **2016**, *7*, No. 11105.
(31) Gong, J.; Yang, M.; Rebollar, D.; Rucinski, J.; Liveris, Z.; Zhu, K.; Xu, T. Divalent Anionic Doping in Perovskite Solar Cells for Enhanced Chemical Stability. *Adv. Mater.* **2018**, *30*, No. 1800973.
(32) Wang, Z.-K.; Li, M.; Yang, Y.-G.; Hu, Y.; Ma, H.; Gao, X.-Y.; Liao, L.-S. High Efficiency Pb-In Binary Metal Perovskite Solar Cells. *Adv. Mater.* **2016**, *28*, 6695−6703.
(33) Lau, C. F. J.; Zhang, M.; Deng, X.; Zheng, J.; Bing, J.; Ma, Q.; Kim, J.; Hu, L.; Green, M. A.; Huang, S.; Ho-Baillie, A. Strontium-Doped Low-Temperature-Processed $CsPbI_2Br$ Perovskite Solar Cells. *ACS Energy Lett.* **2017**, *2*, 2319−2325.
(34) Li, M.; Wang, Z.-K.; Zhuo, M.-P.; Hu, Y.; Hu, K.-H.; Ye, Q.-Q.; Jain, S. M.; Yang, Y.-G.; Gao, X.-Y.; Liao, L.-S. Pb-Sn-Cu Ternary Organometallic Halide Perovskite Solar Cells. *Adv. Mater.* **2018**, *30*, No. 1800258.
(35) Xu, W.; Zheng, L.; Zhang, X.; Cao, Y.; Meng, T.; Wu, D.; Liu, L.; Hu, W.; Gong, X. Efficient Perovskite Solar Cells Fabricated by Co Partially Substituted Hybrid Perovskite. *Adv. Energy Mater.* **2018**, *8*, No. 1703178.
(36) Swarnkar, A.; Mir, W. J.; Nag, A. Can B-Site Doping or Alloying Improve Thermal- and Phase-Stability of All-Inorganic $CsPbX_3$ (X = Cl, Br, I) Perovskites? *ACS Energy Lett.* **2018**, *3*, 286−289.
(37) Lu, M.; Zhang, X.; Zhang, Y.; Guo, J.; Shen, X.; Yu, W. W.; Rogach, A. L. Simultaneous Strontium Doping and Chlorine Surface Passivation Improve Luminescence Intensity and Stability of $CsPbI_3$ Nanocrystals Enabling Efficient Light-Emitting Devices. *Adv. Mater.* **2018**, *30*, No. 1804691.
(38) Jena, A. K.; Kulkarni, A.; Sanehira, Y.; Ikegami, M.; Miyasaka, T. Stabilization of α-$CsPbI_3$ in Ambient Room Temperature Conditions by Incorporating Eu into $CsPbI_3$. *Chem. Mater.* **2018**, *30*, 6668−6674.
(39) Zhou, Y.; Kwun, J.; Garces, H. F.; Pang, S.; Padture, N. P. Observation of Phase-Retention Behavior of the $HC(NH_2)_2PbI_3$ Black Perovskite Polymorph upon Mesoporous TiO_2 Scaffolds. *Chem. Commun.* **2016**, *52*, 7273−7275.
(40) Lehner, A. J.; Fabini, D. H.; Evans, H. A.; Hébert, C.-A.; Smock, S. R.; Hu, J.; Wang, H.; Zwanziger, J. W.; Chabinyc, M. L.; Seshadri, R. Crystal and Electronic Structures of Complex Bismuth Iodides $A_3Bi_2I_9$ (A = K, Rb, Cs) Related to Perovskite: Aiding the Rational Design of Photovoltaics. *Chem. Mater.* **2015**, *27*, 7137−7148.
(41) Chen, C.; Liu, D.; Zhang, B.; Bi, W.; Li, H.; Jin, J.; Chen, X.; Xu, L.; Song, H.; Dai, Q. Carrier Interfacial Engineering by Bismuth Modification for Efficient and Thermoresistant Perovskite Solar Cells. *Adv. Energy Mater.* **2018**, *8*, No. 1703659.
(42) Ahn, N.; Son, D.-Y.; Jang, I.-H.; Kang, S. M.; Choi, M.; Park, N.-G. Highly Reproducible Perovskite Solar Cells with Average Efficiency of 18.3% and Best Efficiency of 19.7% Fabricated via Lewis Base Adduct of Lead(II) Iodide. *J. Am. Chem. Soc.* **2015**, *137*, 8696−8699.
(43) Forney, C. F.; Brandl, D. G. Control of Humidity in Small Controlled-Environment Chambers Using Glycerol-Water Solutions. *HortTechnology* **1992**, *2*, 52−54.
(44) Starcoat T5 High Efficiency and High Output, 2013.
(45) Thomas, A. G.; Joanne, C. Z.; Benjamin, K. T. Spectrophotometry: Accurate Measurement of Optical Properties of Materials. In *Experimental Methods in the Physical Sciences*; Elsevier Science: Waltham, MA, 2014; Vol. *46*.
(46) Abdelhady, A. L.; Saidaminov, M. I.; Murali, B.; Adinolfi, V.; Voznyy, O.; Katsiev, K.; Alarousu, E.; Comin, R.; Dursun, I.; Sinatra, L.; et al. Heterovalent Dopant Incorporation for Bandgap and Type Engineering of Perovskite Crystals. *J. Phys. Chem. Lett.* **2016**, *7*, 295−301.
(47) Zhou, Y.; Yong, Z.-J.; Zhang, W.; Ma, J.-P.; Sadhanala, A.; Chen, Y.-M.; Liu, B.-M.; Zhou, Y.; Song, B.; Sun, H.-T. Ultra-Broadband Optical Amplification at Telecommunication Wavelengths Achieved by Bismuth-Activated Lead Iodide Perovskites. *J Mater. Chem. C* **2017**, *5*, 2591−2596.
(48) Yamada, Y.; Hoyano, M.; Akashi, R.; Oto, K.; Kanemitsu, Y. Impact of Chemical Doping on Optical Responses in Bismuth-Doped

DOI: 10.1021/acs.jpcc.8b11674
J. Phys. Chem. C 2019, 123, 963−970

$CH_3NH_3PbBr_3$ Single Crystals: Carrier Lifetime and Photon Recycling. *J. Phys. Chem. Lett.* **2017**, *8*, 5798−5803.
(49) Nayak, P. K.; Sendner, M.; Wenger, B.; Wang, Z.; Sharma, K.; Ramadan, A. J.; Lovrinčić, R.; Pucci, A.; Madhu, P. K.; Snaith, H. J. Impact of Bi^{3+} Heterovalent Doping in Organic−Inorganic Metal Halide Perovskite Crystals. *J. Am. Chem. Soc.* **2018**, *140*, 574−577.
(50) Mosconi, E.; Merabet, B.; Meggiolaro, D.; Zaoui, A.; De Angelis, F. First-Principles Modeling of Bismuth Doping in the $MAPbI_3$ Perovskite. *J. Phys. Chem. C* **2018**, *122*, 14107−14112.
(51) Lozhkina, O. A.; Murashkina, A. A.; Shilovskikh, V. V.; Kapitonov, Y. V.; Ryabchuk, V. K.; Emeline, A. V.; Miyasaka, T. Invalidity of Band-Gap Engineering Concept for Bi^{3+} Heterovalent Doping in $CsPbBr_3$ Halide Perovskite. *J. Phys. Chem. Lett.* **2018**, *9*, 5408−5411.
(52) Zhang, Z.; Ren, L.; Yan, H.; Guo, S.; Wang, S.; Wang, M.; Jin, K. Bandgap Narrowing in Bi-Doped $CH_3NH_3PbCl_3$ Perovskite Single Crystals and Thin Films. *J. Phys. Chem. C* **2017**, *121*, 17436−17441.
(53) Zhou, Y.; Yong, Z.-J.; Zhang, K.-C.; Liu, B.-M.; Wang, Z.-W.; Hou, J.-S.; Fang, Y.-Z.; Zhou, Y.; Sun, H.-T.; Song, B. Ultrabroad Photoluminescence and Electroluminescence at New Wavelengths from Doped Organometal Halide Perovskites. *J. Phys. Chem. Lett.* **2016**, *7*, 2735−2741.
(54) Zhang, J.; Shang, M.; Wang, P.; Huang, X.; Xu, J.; Hu, Z.; Zhu, Y.; Han, L. N-Type Doping and Energy States Tuning in $CH_3NH_3Pb_{1-x}Sb_{2x/3}I_3$ Perovskite Solar Cells. *ACS Energy Lett.* **2016**, *1*, 535−541.
(55) Wang, J. T.-W.; Wang, Z.; Pathak, S.; Zhang, W.; deQuilettes, D. W.; Wisnivesky-Rocca-Rivarola, F.; Huang, J.; Nayak, P. K.; Patel, J. B.; et al. Efficient Perovskite Solar Cells by Metal Ion Doping. *Energy Environ. Sci.* **2016**, *9*, 2892−2901.
(56) Naumkin, A. V.; Kraut-Vass, A.; Gaarenstroom, S. W.; Powell, C. J. *NIST X-Ray Photoelectron Spectroscopy Database*, NIST Standard Reference Database Number 20; National Institute of Standards and Technology: Gaithersburg, MD, 2000.
(57) Ferreira da Silva, A.; Veissid, N.; An, C. Y.; Pepe, I.; Barros de Oliveira, N.; Batista da Silva, A. V. Optical Determination of the Direct Bandgap Energy of Lead Iodide Crystals. *Appl. Phys. Lett.* **1996**, *69*, 1930−1932.
(58) Li, Y.; Xu, X.; Wang, C.; Ecker, B.; Yang, J.; Huang, J.; Gao, Y. Light-Induced Degradation of $CH_3NH_3PbI_3$ Hybrid Perovskite Thin Film. *J. Phys. Chem. C* **2017**, *121*, 3904−3910.
(59) Manshor, N. A.; Wali, Q.; Wong, K. K.; Muzakir, S. K.; Fakharuddin, A.; Schmidt-Mende, L.; Jose, R. Humidity versus Photo-Stability of Metal Halide Perovskite Films in a Polymer Matrix. *Phys. Chem. Chem. Phys.* **2016**, *18*, 21629−21639.
(60) Xu, W.; Liu, L.; Yang, L.; Shen, P.; Sun, B.; McLeod, J. A. Dissociation of Methylammonium Cations in Hybrid Organic−Inorganic Perovskite Solar Cells. *Nano Lett.* **2016**, *16*, 4720−4725.
(61) Merdasa, A.; Bag, M.; Tian, Y.; Källman, E.; Dobrovolsky, A.; Scheblykin, I. G. Super-Resolution Luminescence Microspectroscopy Reveals the Mechanism of Photoinduced Degradation in $CH_3NH_3PbI_3$ Perovskite Nanocrystals. *J. Phys. Chem. C* **2016**, *120*, 10711−10719.
(62) Avrami, M. Kinetics of Phase Change. I General Theory. *J. Chem. Phys.* **1939**, *7*, 1103−1112.
(63) Christian, J. W. *The Theory of Transformations in Metals and Alloys*; Elsevier Science: Kidlington, Oxford, 2002.
(64) Aristidou, N.; Eames, C.; Islam, M. S.; Haque, S. A. Insights into the Increased Degradation Rate of $CH_3NH_3PbI_3$ Solar Cells in Combined Water and O_2 Environments. *J. Mater. Chem. A* **2017**, *5*, 25469−25475.
(65) Halder, A.; Choudhury, D.; Ghosh, S.; Subbiah, A. S.; Sarkar, S. K. Exploring Thermochromic Behavior of Hydrated Hybrid Perovskites in Solar Cells. *J. Phys. Chem. Lett.* **2015**, *6*, 3180−3184.

DOI: 10.1021/acs.jpcc.8b11674
J. Phys. Chem. C 2019, 123, 963−970